Pergamon

PII: S0191-8141(97)00059-X

Journal of Structural Geology, Vol. 20, No. 2/3, pp. 195 to 209, 1998

0191-8141/98 $19.00 + 0.00

Mechanisms of shear localization in the continental lithosphere: inference from the deformation microstructures of peridotites from the Ivrea zone, northwestern Italy

DENGHUI JIN* and SHUN-ICHIRO KARATO

Department of Geology and Geophysics, University of Minnesota, Minneapolis, MN 55455, U.S.A.

and

MASAAKI OBATA

Department of Geology, Kumamoto University, Kurokami, Kumamoto 860, Japan

(*Received* 17 *February* 1997; *accepted in revised form* 23 *July* 1997)

Abstract—The ultramafic massif of Balmuccia, northwestern Italy, shows a variety of deformation fabrics including some localized shear zones that resulted in nearly complete melting (pseudotachylyte). A series of peridotite specimens were collected near one of the pseudotachylyte fault veins to investigate the mechanisms of shear localization. The microstructural analyses show at least three deformation stages. The first (stage I) is nearly homogeneous deformation at low stress (~3 MPa) and high temperature (~1300–1500 K), followed by localized deformation (stage II) at a higher stress (~60 MPa) and moderate temperature (~1000–1150 K) and, finally, semi-brittle deformation (stage III) at a very high stress (~400 MPa) that resulted in the formation of pseudotachylyte. The stage II deformation resulted in relatively small strains in most areas but significant localized deformation leading to dynamic recrystallization occurred, the degree of which increases systematically toward the fault zone. Based on this observation, together with the observation that the brittle deformation post-dated dynamic recrystallization, we conclude that the shear localization in this locality occurred as a result of ductile deformation rather than brittle deformation. Various mechanisms of shear localization in the ductile regime are examined and we conclude that the grain-size reduction due to dynamic recrystallization at relatively high stresses and moderate temperatures is a probable mechanism of shear localization. The intermediate regime between dislocation and diffusion creep, where rheology is grain-size-sensitive yet continuous recrystallization occurs due to dislocation creep, is suggested to play an important role in shear localization in the upper mantle. The conditions of shear localization due to this mechanism are examined based on the laboratory data on creep and dynamic recrystallization. It is shown that shear localization occurs at relatively low temperatures and/or high stresses. Localized deformation in the continental lithosphere will occur well below the brittle–ductile transition (~10 km depth), down to ~40–80 km depth depending upon the geothermal gradient and water fugacity. © 1998 Elsevier Science Ltd.

INTRODUCTION

Localization of deformation is ubiquitous in the lithosphere, and the understanding of the extent to which localization occurs is an important issue in the dynamics of the lithosphere. In fact, one of the most important characteristics of deformation associated with plate tectonics is strain localization. Such localized deformation does not occur in the convecting simple viscous fluid. Localized deformation occurs as a result of unique rheological properties of Earth materials, but the conditions under which localized deformation could occur have not been well understood.

The mechanical behavior of the lithosphere includes brittle deformation in its shallow portions and ductile deformation in the deeper portions. Brittle deformation occurs in a localized manner in most cases and hence the strength of the lithosphere in the shallow portions is determined by the resistance to fault motion (e.g. Goetze and Evans, 1979). Localization in the brittle regime is due to the coalescence of microcracks and is well documented (e.g. Paterson, 1978). In contrast, deformation in the ductile regime usually occurs more or less homogeneously, but under some conditions localized deformation does occur (e.g. Poirier, 1980; White *et al.*, 1980; Hobbs *et al.*, 1986; Handy, 1989; Drury *et al.*, 1991; Vissers *et al.*, 1995; Jaroslow *et al.*, 1996). When deformation is localized in the ductile regime, the strength of rocks is largely controlled by the strength of localized 'fault' regions and may be significantly lower than that corresponding to a homogeneous deformation.

The brittle–ductile transition in the continental lithosphere occurs at ~10 km depth, whereas the thickness of the continental lithosphere exceeds ~50 km (e.g. Kohlstedt *et al.*, 1995) and could be as thick as ~200–400 km (e.g. Jordan, 1975; Peltier, 1984). Therefore, localization in the ductile regime plays an important role in the deformation of the continental lithosphere. However, the mechanisms and the extent of localization in the ductile regime are poorly understood (e.g. Poirier, 1980; White *et al.*, 1980; Hobbs *et al.*, 1986; Handy, 1989; Drury *et al.*, 1991; Vissers *et al.*, 1995; Jaroslow *et al.*, 1996).

*Present address: Department of Computer Sciences, Iowa State University, Ames, IA 50011, U.S.A.

The Balmuccia peridotite massif of the Ivrea zone, northwestern Italy, provides a good opportunity to investigate the mechanisms of shear localization. This peridotite massif, and also the surrounding basic and silicic rocks, show spectacular evidence of plastic deformation including localized deformation at high stress levels (Brodie and Rutter, 1987; Rutter and Brodie, 1988, 1990; Skrotzki *et al.*, 1990; Techmer *et al.*, 1992; Rutter *et al.*, 1993; Obata and Karato, 1995). In some localities, the localized deformation led to melting along the faults forming pseudotachylytes (Techmer *et al.*, 1992; Obata and Karato, 1995). Skrotzki *et al.* (1990) and Obata and Karato (1995) made microstructural and petrological analyses of ultramafic rocks from this region and found evidence for high stress deformation. Based on the observations of dislocation microstructures, Skrotzki *et al.* (1990) inferred a two-stage deformation history: low stress–high temperature deformation, followed by high stress–low temperature deformation. Based on petrological and microstructural observations, Obata and Karato (1995) found evidence for rapid and hence nearly adiabatic deformation resulting in almost complete melting of fault-zone peridotites and suggested that the pseudotachylyte was formed by an ancient upper mantle earthquake. Thus, localized deformation has been well recognized in this region, but the mechanisms of shear localization remain poorly understood.

To investigate the mechanisms of shear localization a series of specimens from one of the pseudotachylyte fault veins were collected and their microstructures were examined using an optical microscope, a scanning electron microscope (SEM) and a transmission electron microscope (TEM).

GEOLOGICAL SETTING AND SAMPLES

The geological setting and outline of the Balmuccia peridotite have been described in previous studies (Shervais, 1979; Boudier *et al.*, 1984; Rutter and Brodie, 1990; Skrotzki *et al.*, 1990; Zingg *et al.*, 1990; Rutter *et al.*, 1993; Obata and Karato, 1995) and only a brief summary is given below. The Balmuccia peridotite is a mantle-derived spinel lherzolite massif and occurs in the western margin of the Ivrea zone of northwestern Italy, near the Insubric line (Fig. 1). The Ivrea zone, a NNE- to NE-trending elongated terrain of metamorphic–igneous complex, is thought to represent a cross-section of the lowermost continental crust and the uppermost mantle of the South Alpine plate. The metamorphic grade varies from amphibolite in the east to granulite in the west, and the temperature (T)–pressure (P) conditions of the metamorphism around the peridotite are estimated to be $T = 1000$–1150 K and $P = 0.9$–1.1 GPa (Schmid and Wood, 1976). The dominant rock type in the Balmuccia peridotite is a medium- to coarse-grained spinel lherzolite composed of ~60% olivine, ~25% orthopyroxene,

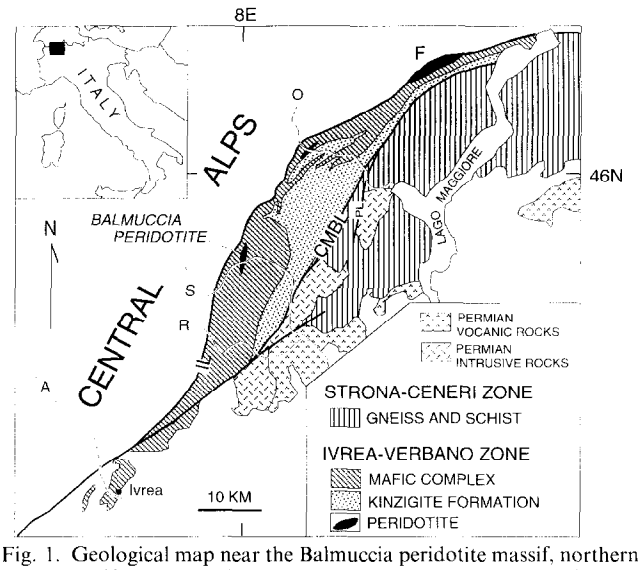

Fig. 1. Geological map near the Balmuccia peridotite massif, northern Italy (modified from Obata and Karato, 1995). IL, Insubric line; CMBL, Cossate–Mergozzo–Brissago line; PL, Poggallo line; F, Finero peridotite; A, Aosta Valley; R, Sessera Valley; S, Sesia Valley; O, Ossola Valley.

~10% of clinopyroxene, ~5% spinel and a trace amount of hornblende (Shervais, 1979; Boudier *et al.*, 1984; Skrotzki *et al.*, 1990; Obata and Karato, 1995). Cataclastic deformation and mylonites are found near the western contact zone. Two types of pyroxenite layer or dykes occur; one is the Cr-diopside layers characterized by bright green, chrome-rich, aluminum-poor clinopyroxene; another is the Al-augite suite characterized by a gray, chrome-poor, alumina-rich clinopyroxene. The Cr-diopside layers usually show significant penetrative deformation and are nearly concordant to primary layering of the peridotite, while the Al-augite type is less deformed and typically cross-cuts the Cr-diopside layers. The equilibration temperature and pressure of the peridotite have been estimated using geothermo-barometers and phase equilibrium constraints to be $T = 1300$–1500 K and $P = 1.3$–2.0 GPa (Shervais, 1979).

The regional foliation in the peridotite massif is dipping steeply to the west (Boudier *et al.*, 1984). Its trend is ~N5°E and the dip is ~85° to the west in the southern portion where the samples were collected. The spinel lineation plunges ~50–60° to N5°E. The pseudotachylyte layer examined is a fault-vein type defined by Sibson (1975) that occurs on a bank of the Sesia River. It is the same shear zone described in Obata and Karato (1995). The layer is nearly vertical and straight (the width is up to 3 cm), trending N40–50°E (Fig. 2). The displacement along the fault has been measured using the offset of the pyroxenite layers that are cross-cut by the fault. Twelve core samples were collected, using a portable core picker, across this layer at various distances from the fault vein (Fig. 2b) and thin sections were made.

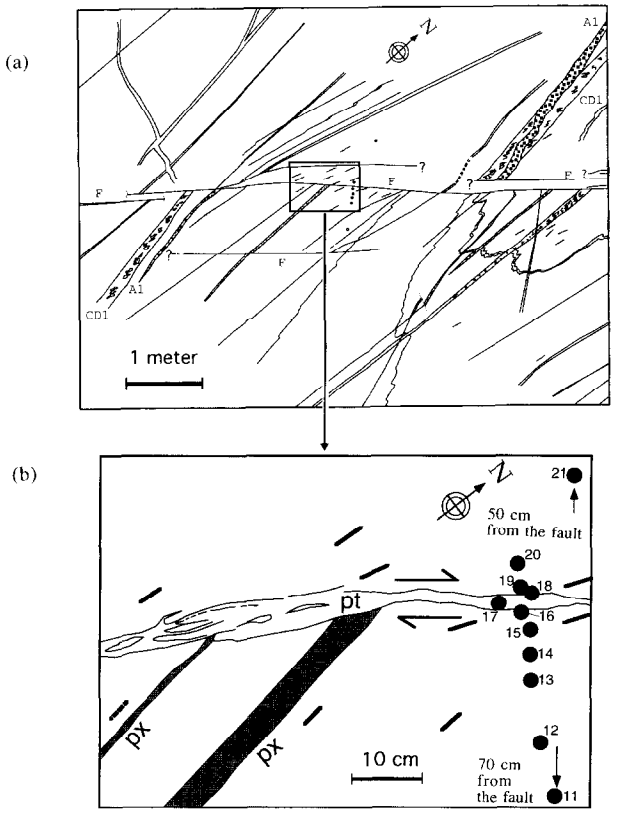

Fig. 2. (a) A field sketch of a fault-vein type pseudotachylyte layer outcrop on the Sesia river. The outcrop surface is nearly horizontal and the sketch is a planar view looking down. F, fault vein filled with pseudotachylyte. Al, aluminum-rich augite pyroxenite layer. CD1, a chromium-diopside pyroxenite layer. About a 3 m horizontal displacement can be estimated from the offset of pyroxenite layers. (b) The sampling locations of peridotites near the pseudotachylyte vein. Circles indicate core positions and the numbers show the specimen numbers. Thick bars indicate the trace of foliation plane which is nearly vertical. pt, pseudotachylyte vein; px, pyroxenite dyke. The sense of shear inferred from the offset of a pyroxenite dyke is indicated by arrows.

MICROSTRUCTURES

General: recrystallization and cracking

Optical micrographs of some of the ultramafic rocks from the Balmuccia peridotite massif are shown in Fig. 3. These rocks show a porphyroclastic microstructure characterized by bimodal grain-size distribution (coarse grains 2–4 mm and fine grains 30–60 μm in most cases, but in the vicinity of the fault grain size becomes only a few μm). Fine grains (neoblasts) are mostly olivine. Coarse grains (porphyroclasts) show a moderately strong foliation or lineation defined by grain-shape elongation and spinel alignment. Foliation or lineation in samples far from the fault agree well with those described by Boudier *et al.* (1984). Close to the fault, foliation and lineation are affected by local deformation, and the foliation plane becomes close to the fault plane (see also Fig. 2b). However, due to the significant effects of cataclastic deformation, precise identification of foliation or lineation near the fault is difficult.

Undulatory extinction and subgrains are ubiquitous. Along the grain boundaries of porphyroclasts, much smaller grains of olivine (neoblasts) are observed that show some elongation but less undulatory extinction. Recrystallization is less extensive in orthopyroxene and clinopyroxene. Coarse grains of olivine show evidence for high-stress deformation including kink bands. Orthopyroxene shows fine-scale lamellae of clinopyroxene with identical chemical composition indicating deformation under high stresses (Coe and Kirby, 1975; Skrotzki *et al.*, 1990).

Evidence for dynamic recrystallization by both subgrain rotation (Fig. 4a) and grain-boundary migration (Fig. 4b) is seen in many olivine grains. The percentage of recrystallization was measured from thin sections using NIH image analysis software. The fraction of recrystallized grains increases systematically toward the fault (Fig. 5). The recrystallized grain size is heterogeneous, but remains almost constant up to very close to the fault. In the very vicinity of the fault (e.g. samples 16 and 18), a dramatic reduction of grain size to ~ 5 μm is observed (Fig. 6).

Cracking is also ubiquitous, but the density of cracks increases toward the fault. In many cases, cracks cut coarse grains (porphyroclasts; Fig. 7a) and fine-grained recrystallized regions (Fig. 7b). This observation clearly indicates that the brittle deformation post-dates the deformation event responsible for dynamic recrystallization and deformation of coarse grains.

Lattice-preferred orientation (LPO)

The lattice-preferred orientation of olivine was measured using a U-stage. The results are plotted using equal-area projection on a lower hemisphere. The foliation or lineation (see Fig. 2) is used as a reference frame. The orientation of the pseudotachylyte vein is also shown for comparison. Measurements were made separately for the coarse grains (porphyroclasts) and small grains (neoblasts). When the percentage of recrystallization is small, the LPO of fine grains is measured from various portions of a specimen, and the results are added. In samples far from the fault (BM-11 and -12), the LPO is strong and is characterized by a strong [010] peak perpendicular to the foliation plane and a less strong but appreciable [100] peak nearly parallel to the lineation (Fig. 8a). The LPO is significantly modified in samples within ~ 10 cm of the fault (e.g. BM-18).

The LPO of fine-grained olivine is similar to that of the coarse-grained olivine in samples far from the fault (BM-11). However, the LPO of fine-grained olivine becomes distinct from that of coarse-grained counterparts near the fault. The LPO of fine-grained olivines shows a strong [001] maximum, and diffuse [100] and [001] peaks, sometimes with subpeaks (BM-18) (Fig. 8b).

Dislocation microstructures

The dislocation microstructures in olivine were analyzed under an optical microscope or a scanning electron

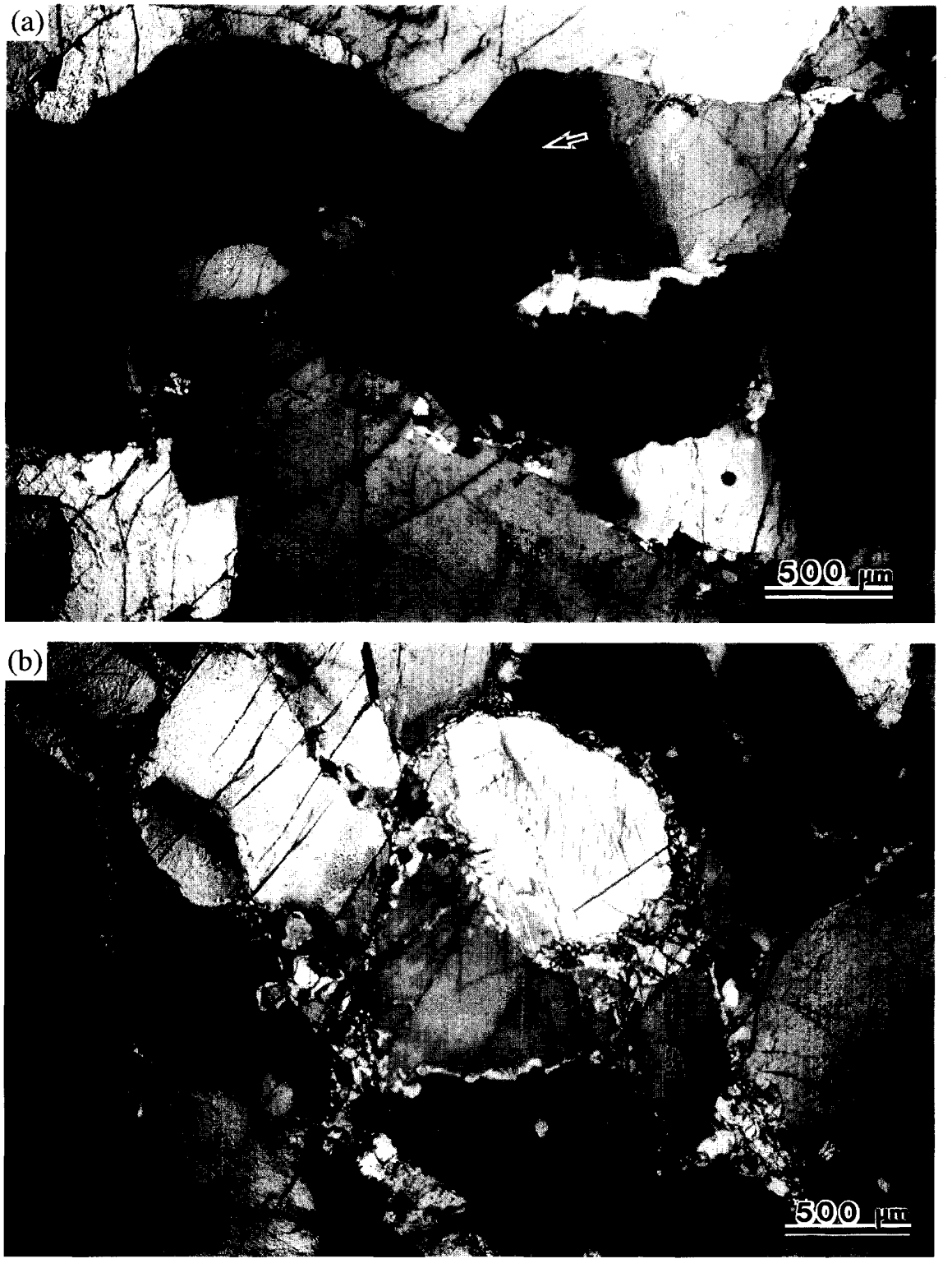

Fig. 3. Optical micrographs of samples (all crossed nicols). (a) Sample BM-11, 70 cm away from pseudotachylyte vein (fault). Very little recrystallization is observed, although evidence of high stress deformation is clear from kink bands in olivine (shown by an arrow). (b) Sample BM-13, 8 cm from the pseudotachylyte vein. The degree of recrystallization is significantly higher than that in a sample further from the pseudotachylyte vein.

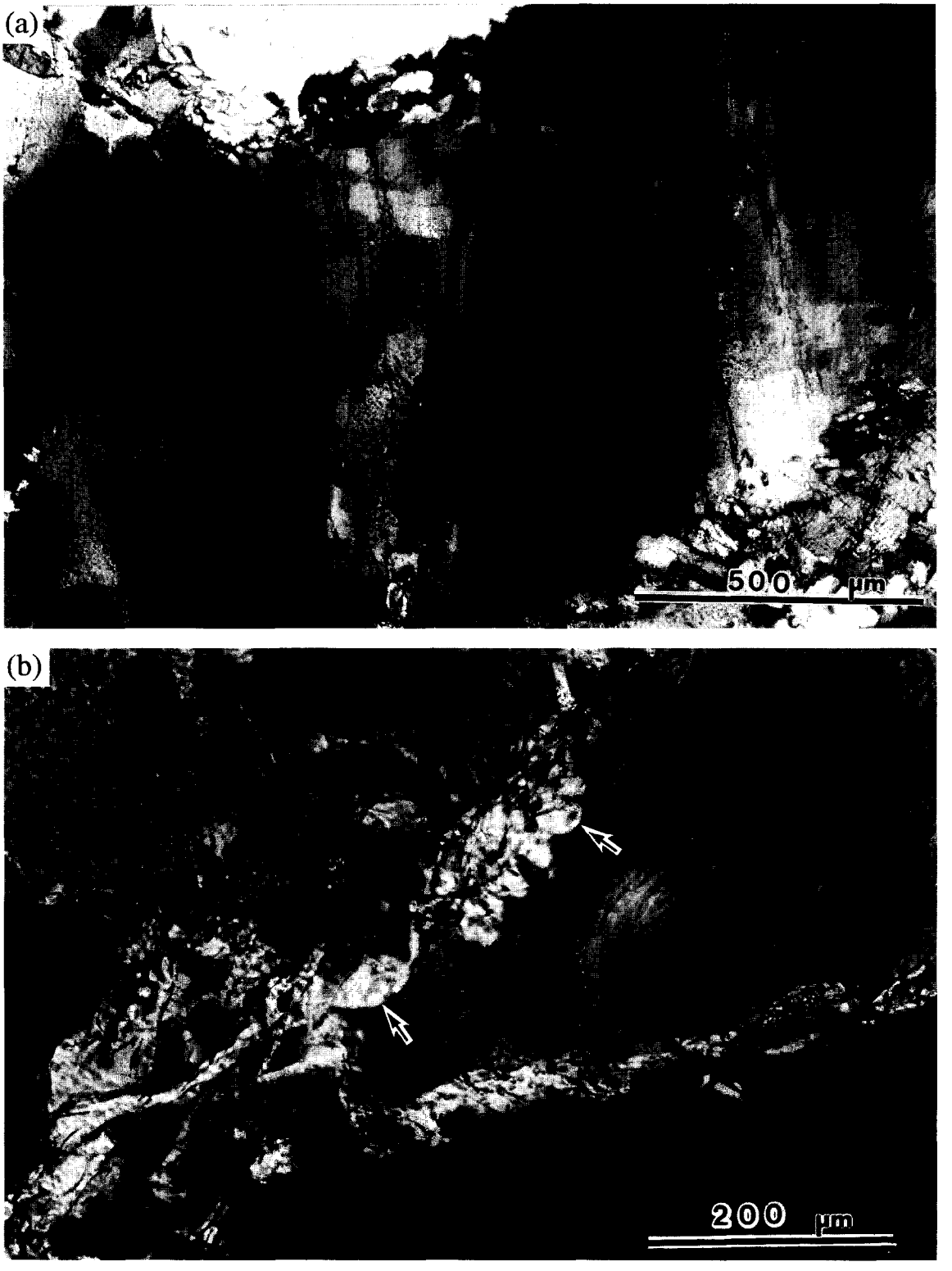

Fig. 4. Optical micrographs showing dynamic recrystallization. (a) Sample BM-15, 3 cm from the pseudotachylyte vein. An olivine grain shows clear evidence for subgrain rotation. Subgrain boundaries are mostly on (100) and (001) planes. (b) Sample BM-13, 8 cm from the pseudotachylyte vein. Evidence of grain-boundary migration is seen (arrows indicate grain boundaries that are likely to have been migrating due to the gradient in dislocation density, see also Fig. 9c).

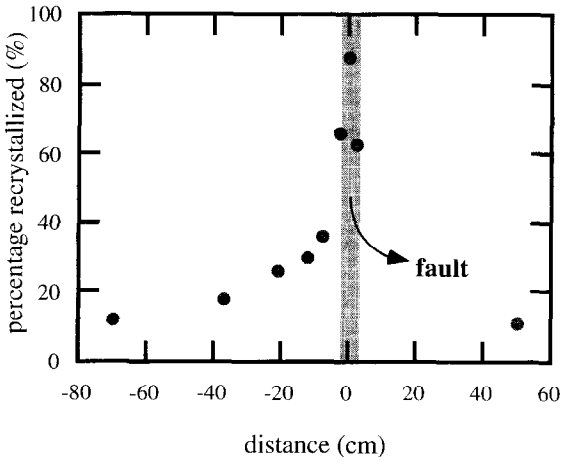

Fig. 5. Percentage of recrystallized grains as a function of distance from the fault.

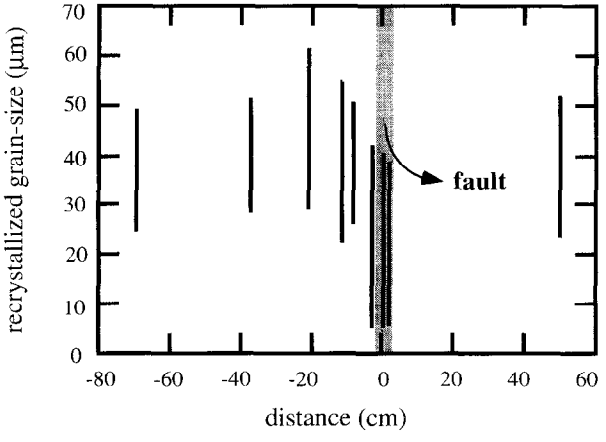

Fig. 6. Recrystallized grain size as a function of distance from the fault. The size of recrystallized grains from about 10 to 20 grain boundaries were measured to obtain a range of recrystallized grain size. The intercept method was used to estimate grain size using a correction factor of 1.5.

microscope with a back-scattered electron imaging mode (Karato, 1987) using the oxidation decoration technique or a transmission electron microscope. The results of SEM observations are shown in Fig. 9. The dislocation density is nearly homogeneous and very few areas of low dislocation density were found. However, in other regions, dislocation densities are markedly different and the grain boundaries are concave toward a high dislocation density side (Fig. 9c), indicating that fast grain-boundary migration occurred driven by the difference in dislocation density (e.g. Karato, 1988). Dislocation density in most portions of the specimens is $\sim 10^{12}\ m^{-2}$ and abundant subgrain boundaries are observed. Many of the subgrain boundaries are (001) tilt boundaries, but (100) tilt boundaries are also observed (Fig. 9a & b). The TEM observations indicate that the dominant Burger's vector is [001] with some [100] as well (Skrotzki *et al.*, 1990; Obata and Karato, 1995), and that the dislocation density increases to $\sim 10^{13}\ m^{-2}$ in the close ($\sim$2–3 cm) vicinity to the pseudotachylyte fault vein (Obata and Karato, 1995).

DISCUSSION

Deformation history

Three stages of deformation can be recognized.

Stage I. The deformation event associated with coarse-grained portions. The observation of a significant LPO in the coarse-grained portions indicates that deformation of this portion was accommodated by dislocation creep (Karato, 1988, 1989a) to a significant strain ($\sim$50% or more; Zhang and Karato, 1995). Thus, we assume that the grain size (2–4 mm) in the rock is determined by the applied stress. Using the dynamically recrystallized grain-size piezometer calibrated by Karato *et al.* (1980) (see also van der Wal *et al.*, 1993) it was estimated that the stress associated with this event was $\sim 3 \pm 1$ MPa.

Stage II. A transitional microstructure, such as that shown in Fig. 3(b), suggests that the dynamic recrystallization followed the deformation of coarse grains. The percentage of recrystallization increases toward the fault, indicating that strain associated with this event increases toward the fault. The deformation event associated with the formation of small recrystallized grains occurred at higher stresses. Again, using Karato *et al.* (1980) (or van der Wal *et al.*, 1993), the stress level was estimated to be $\sim 60 \pm 20$ MPa.

Stage III. Finally, brittle or semi-brittle deformation that is presumably associated with pseudotachylyte formation occurred. Cracks cut coarse porphyroclasts and fine neoblasts, which indicates that the cracking occurred after dynamic recrystallization (Fig. 7). Microstructures of rocks within $\sim$2–3 cm of the fault zone suggest a significantly higher stress level than that associated with dynamic recrystallization in rocks far from the fault. For example, the very small size of dynamically recrystallized grains ($\sim 5\ \mu m$) and a high dislocation density ($\sim 10^{13}\ m^{-2}$) (Obata and Karato, 1995) suggest that stresses during stage III were $\sim 400 \pm 200$ MPa.

The correspondence of this deformation history with geological history of this area is not clear. One possibility is that the first stage of low stress and high temperature deformation occurred at 40–60 km depth at $T = 1300$–1500 K, where the lherzolite assumed chemical equilibrium. This temperature–depth relationship implies a rather high geothermal gradient corresponding to a heat flow of $\sim$80–120 mW m^{-2}, and hence suggests a rifting event that is considered to have occurred during the Caledonian (Shervais, 1979; Boudier *et al.*, 1984). The second stage of moderate temperature and higher stress deformation could be related to a tectonic event(s) that caused granulite-facies metamorphism (uplifting), which was probably associated with the emplacement of this rock mass. The final, very high, stress event presumably

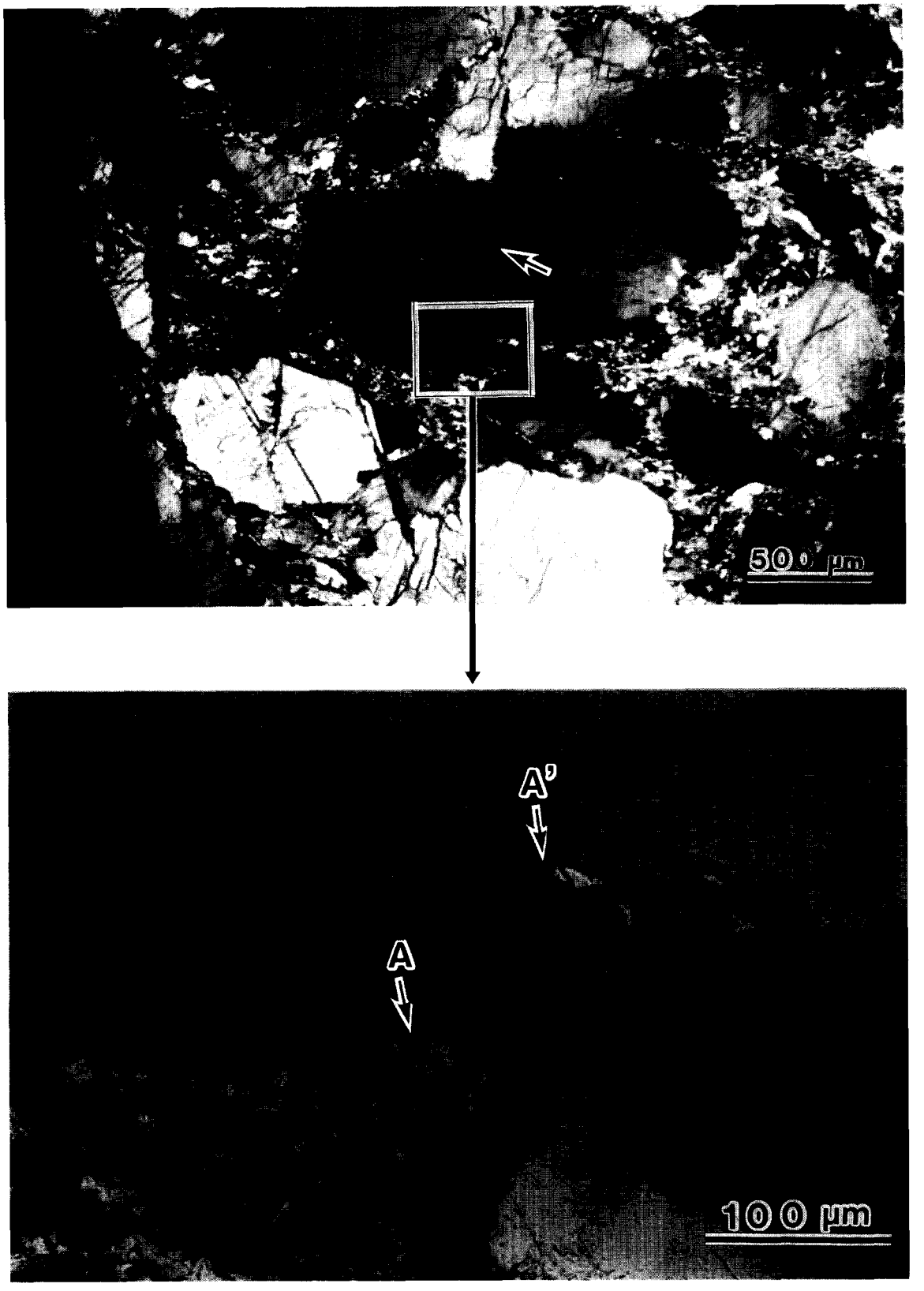

Fig. 7. Optical micrographs of a sample (BM-18) close to the pseudotachylyte vein (all crossed nicols), showing both ductile and brittle deformation. (a) Cracks cut both large grains and zones of recrystallized grains (a microfault is shown by an arrow). (b) Close-up of the rectangular area in (a) showing that a recrystallized grain was cut into two halves (A and A') by a fault, indicating that the faulting occurred after dynamic recrystallization.

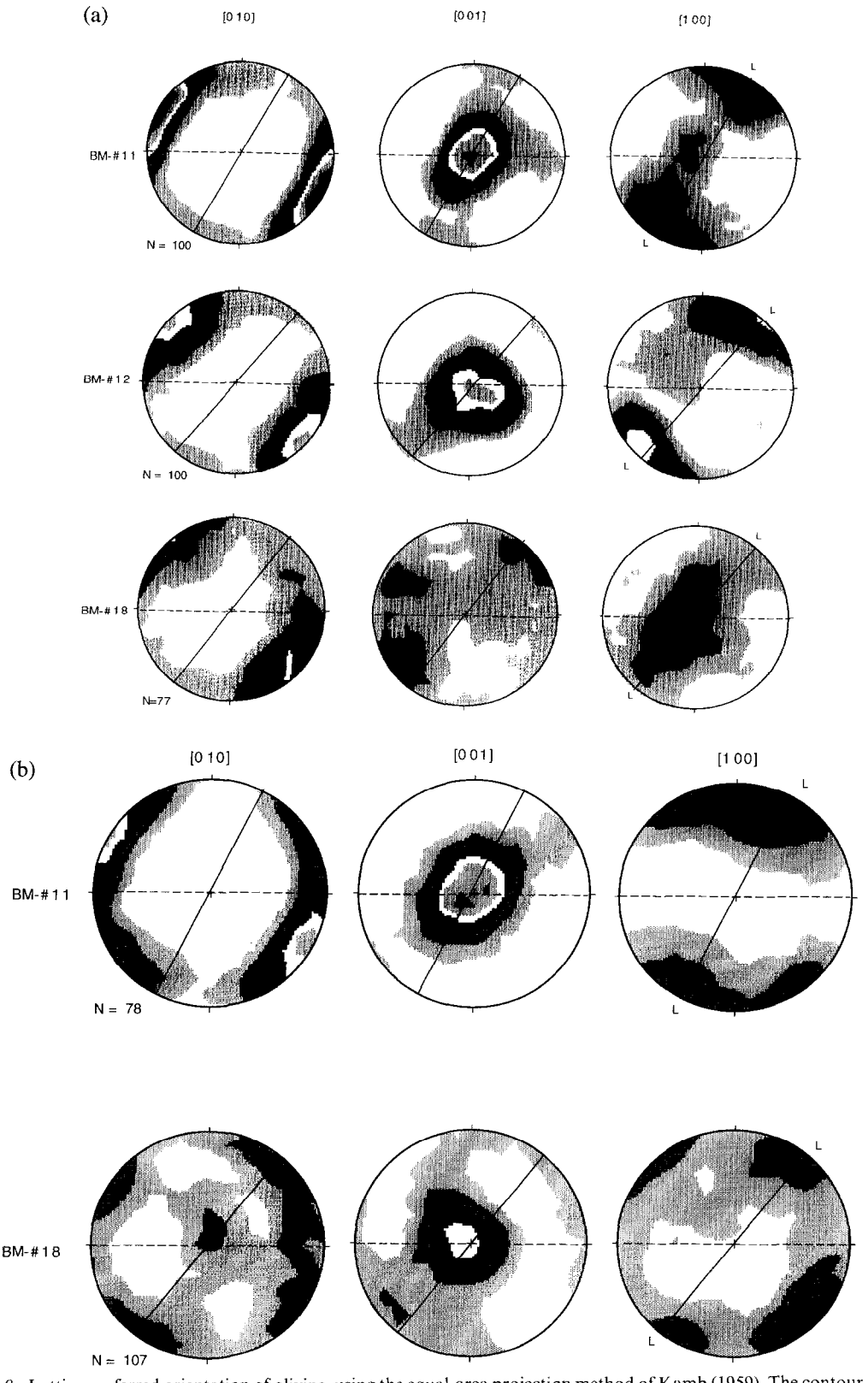

Fig. 8. Lattice-preferred orientation of olivine, using the equal-area projection method of Kamb (1959). The contour interval is 2σ (standard deviation). The solid lines indicate the trace of the foliation plane corresponding to regional-scale deformation and L indicates regional lineation as determined by Boudier *et al.* (1984). The broken lines indicate the trace of the pseudotachylyte vein. (a) Coarse-grained olivine (porphyroclasts). The LPO is strong and has an orthorhombic symmetry ([100] peak parallel to regional lineation and [010] peak perpendicular to regional foliation) in samples far from the pseudotachylyte vein (e.g. BM-11 and -12), whereas LPO becomes diffuse near the vein (e.g. BM-18). (b) Fine-grained recrystallized olivine (neoblasts). The LPO is similar to that of coarse grains in samples far from the vein (BM-11). The LPO of fine-grained olivine becomes diffuse and different from that of coarse-grained olivine near the pseudotachylyte vein (BM-18).

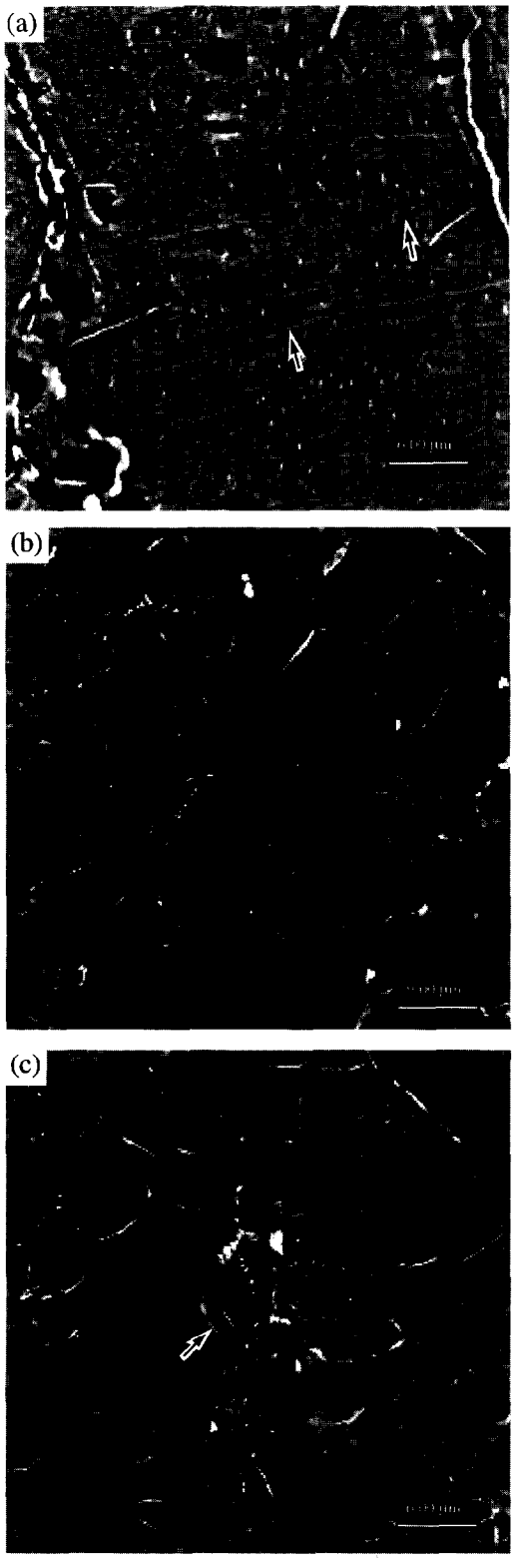

Fig. 9. Dislocation microstructures observed by oxidation decoration with an SEM back-scattered electron imaging technique. (a) Sample BM-16 (a large olivine porphyroclast) showing an homogeneous and high dislocation density. (001) subboundaries are indicated by arrows. (b) Sample BM-16 (olivine neoblasts) showing low contrasts in dislocation density across grain boundaries suggesting a subgrain-rotation mechanism of recrystallization. (c) Sample BM-16 (olivine neoblasts) showing a large contrast in dislocation density suggesting rapid grain-boundary migration (an arrow indicates a grain boundary across which the contrast in dislocation density is high).

occurred in the later stage of emplacement. It is possible that these events occurred during a single series of tectonic events from rifting to subsequent uplifting (Boudier *et al.*, 1984), all of which may ultimately be the result of continental collision. However, the radiometric dating provides constraints only on the time of the metamorphic event.

Deformation mechanisms

The deformation mechanisms for the coarse olivine grains may be inferred from the lattice-preferred orientation (LPO). The LPO of coarse-grained olivine is consistent with the deformation using mostly the [100](010) slip system that dominates under high temperature and low differential stress (e.g. Nicolas and Christensen, 1987; Zhang and Karato, 1995). This slip system is consistent with inferred deformation conditions (low stress ($\sim$3 MPa) and high temperature ($\sim$1300–1500 K)) for the stage I deformation event. The observed diffuseness of LPO close to the fault may reflect the influence of stage II deformation that may have occurred at lower temperatures and at higher stresses. Under these conditions many slip systems in olivine contribute equally to LPO, and the LPO becomes diffuse (Nicolas and Christensen, 1987). In fact, most of the dislocations observed are considered to have been formed during stage II (or III) (Skrotzki *et al.*, 1990; Obata and Karato, 1995).

The similarity of the LPO of fine-grained olivines with coarse-grained counterparts in specimens with a small degree of recrystallization suggests that the fine-grained olivines were formed from coarse ones through subgrain rotation (Poirier and Nicolas, 1975; Karato *et al.*, 1980). In these cases, orientations of new grains largely inherit those of their parent grains, the LPO of which was determined largely by the stage I deformation. However, LPO becomes diffuse close to the fault, which may reflect the fact that the LPO in these regions may be determined by the stage II or III deformation in which many slip systems contribute equally to total strain, hence resulting in a diffuse LPO. Alternatively, significant contribution of grain-boundary sliding in the deformation of fine-grained portions may have caused diffuse LPO. It was noted, however, that the relatively weak LPO of both coarse and fine grains of olivine in the vicinity of the fault zone may in part be the result of the difference in deformation geometry between stage I and stage II, as indicated by the different orientations of foliation or lineation for these two stages (see Fig. 2).

Dislocation structures near many grain boundaries (Fig. 9b) show nearly continuous distribution. However, at other grain boundaries, heterogeneous distribution suggesting fast grain-boundary migration is also seen (Fig. 9c). These observations are similar to what was observed by Karato *et al.* (1980, 1982) and could be attributed to a gradual increase in grain-boundary mobility and/or in dislocation density contrast as the

misfit angle increases during subgrain rotation. The similarity in recrystallization mechanisms between those in experimental specimens and the specimens from Balmuccia peridotite provides support for the use of the experimentally determined recrystallized grain-size piezometer to estimate stress levels.

Mechanisms of shear localization

The deformation microstructures of these rocks suggest a three-stage deformation history. Stage I resulted in large strain as shown by a strong LPO. Strain associated with this stage was nearly homogeneous as inferred from the fairly uniform LPO in the Balmuccia peridotite massif (Boudier *et al.*, 1984). In contrast, the effects of stage II deformation on the LPO are not very great in specimens far from the pseudotachylyte fault vein, although high dislocation densities corresponding to stage II deformation are observed throughout the peridotite massif (Skrotzki *et al.*, 1990). Because a large strain (say $\sim 50\%$ or more) is needed to change LPO (Zhang and Karato, 1995), but only a small strain (say $\sim 1\%$) is required to change dislocation density (Kohlstedt and Goetze, 1974), these observations indicate that the high stress level associated with stage II deformation was present uniformly in this area, but the strain magnitude associated with stage II deformation was in general very small (less than $\sim 10\%$). Large strains only occurred near the fault during stage II deformation. Therefore, deformation corresponding to stage II is considered to have been highly localized. Stage III deformation was also highly localized. Very high dislocation density ($\sim 10^{13}$ m^{-2}) and small recrystallized grains (~ 5 μm) are only observed in the vicinity of the fault (less than ~ 2–3 cm). Therefore, we consider that the high stress in stage III is due to some stress concentration associated with fault motion.

Let us now consider how this localized deformation may have occurred. Mechanisms of shear localization can be classified into two categories: (i) those associated with brittle deformation (due to crack coalescence; Paterson, 1978); and (ii) those associated with ductile deformation. The observation that brittle deformation post-dates dynamic recrystallization and that the percentage of dynamic recrystallization increases toward the fault zone indicates that the brittle fracture is a result of shear localization and not a cause for shear localization. Possible mechanisms of shear localization in the ductile regime include: (1) (localized) grain-size reduction due to dynamic recrystallization (Post, 1977; Karato *et al.*, 1986; Rutter and Brodie, 1988; Handy, 1989); (2) (localized) grain-size reduction due to phase transformations or chemical reactions (Rubie, 1983; Handy, 1989; Vissers *et al.*, 1995); (3) geometrical softening due to LPO (Harren *et al.*, 1988); (4) elimination of work hardening due to grain-boundary migration (Luton and Sellars, 1969; Zeuch, 1982); (5) adiabatic heating (Hobbs *et al.*, 1986; Obata and Karato, 1995); (6) fluid infiltration (Handy, 1989; Drury *et al.*, 1991); and (7) progressive strain partitioning in multiphase materials (Handy, 1989, 1994).

The first mechanism, i.e. localized grain-size reduction due to dynamic recrystallization, has much support from the microstructures here. The percentage of recrystallization systematically increases towards the fault (Fig. 5) and cracks cut recrystallized grains (Fig. 7), indicating that recrystallization occurred first followed by brittle fracture. When material is deformed in the dislocation creep regime (e.g. stage I deformation), grain size at steady state is determined by the recrystallized grain size vs stress relationship. When stress is increased due, for example, to the decrease in temperature or to some tectonic event, such as continental collision, then the grain size corresponding to a new stress will be smaller. Therefore, new small grains will be formed (along grain boundaries). If the size of new grains is small enough, then newly recrystallized portions will be weaker than the rest. Once the volume fraction of this recrystallized portion becomes large enough to form a continuous 'film', then deformation of a partially recrystallized material will occur mostly along these regions. This enhanced deformation leads to further recrystallization, hence shear localization will occur.

The second mechanism is easily ruled out because no phase transformation or chemical reaction is observed. The third mechanism, shear localization due to geometrical softening, is well documented in metallurgy (Harren *et al.*, 1988). This mechanism would imply that the LPO should get stronger as one approaches the fault. This is not the case in this particular shear zone (Fig. 8), and this mechanism may be ruled out. In addition, both numerical modeling (Wenk *et al.*, 1991) and laboratory experiments (Zhang *et al.*, submitted) show that LPO development in olivine may result in hardening rather than softening.

The fourth mechanism implies that moving boundaries result in significant reduction in dislocation density. This mechanism is effective only when work hardening due to increased dislocation density is significant (Luton and Sellars, 1969). Our observation is marginal as to the significance of grain-boundary migration to reduce dislocation densities (Fig. 9b & c). In addition, most experimental studies on olivine showed no significant work hardening (e.g. Kohlstedt and Goetze, 1974; Durham *et al.*, 1985). Therefore, it is considered that this mechanism is unlikely to be important in olivine under these conditions. However, mechanical behavior of peridotites at relatively low temperatures must be better characterized to corroborate this point.

Adiabatic heating to cause localized deformation was discussed by Hobbs *et al.* (1986), and a quantitative analysis of adiabatic heating during the formation of this pseudotachylyte was made by Obata and Karato (1995). However, whether it was responsible for shear localization in stage II or it was important only in stage III is not clear. Considering the much higher stress estimated for

stage III, it is conceivable that adiabatic heating was significant in the latest stage but not much in stage II. We suggest that the localized deformation in stage II triggered thermal runaway, by enhancing strain-rate, causing nearly total melting of this peridotite (Hobbs *et al.*, 1986; Obata and Karato, 1995). The fluid infiltration could possibly cause shear localization if it occurs heterogeneously. However, fluid infiltration is most likely to occur in the brittle regime where permeability of fluid is high. Since the brittle deformation occurred after shear localization, this is considered to be an unlikely mechanism. Evidence for the progressive partitioning of strain from strong to weak minerals is not found in our specimens.

To summarize, we have strong evidence for the weakening due to grain-size reduction as a cause for shear localization. Other mechanisms such as adiabatic heating and fluid infiltration might have contributed to localization, but the evidence to support them is rather weak. One observation that is not consistent with the present interpretation is the rather strong LPO observed for the fine-grained olivine. The operation of grain-size-sensitive diffusion creep or superplastic creep would imply weak or no LPO (Karato, 1988). We offer the following interpretations. (i) The deformation mechanism was diffusion creep, but LPO was formed because of the vicinity of the deformation conditions to the boundary to dislocation creep (Fig. 10b). In fact, Zhang *et al.* (submitted) found significant LPO in samples whose rheology shows evidence of diffusion creep (stress exponent ~ 1, grain-size exponent ~ 2). This is presumably due to the fact that, owing to the distribution of grain size, some portion of a specimen could still deform by dislocation creep although the average rheology is controlled by diffusion creep. (ii) Alternatively, the deformation mechanism in the fine-grained portions may indeed be dislocation creep, yet there is some grain-size effect to reduce the strength. In fact, Hirth and Kohlstedt (1995b) found that the creep strength in the dislocation creep regime is a weak function of grain size near the boundary to diffusion creep. This is presumably due to the change in rate-controlling slip systems, from a hard one ([001](010)) (multi-slip) at the condition far from the boundary, to a soft one ([100](010)) (single slip) near the boundary, caused by the significant effects of diffusion creep and/or grain-boundary sliding to provide accommodation strain near the boundary. It seems that there is a range of deformation conditions close to the boundary between diffusion and dislocation creep in which rheology is sensitive to grain size, yet a significant strain is taken by dislocation glide.

It is proposed that shear localization in this peridotite occurred due to the grain-size reduction caused by dynamic recrystallization, which reduced the grain size enough to make rheology sensitive to grain size, although much of the strain in this regime was probably due to dislocation creep. Such an intermediate deformation regime, where grain-size-sensitive processes help strain

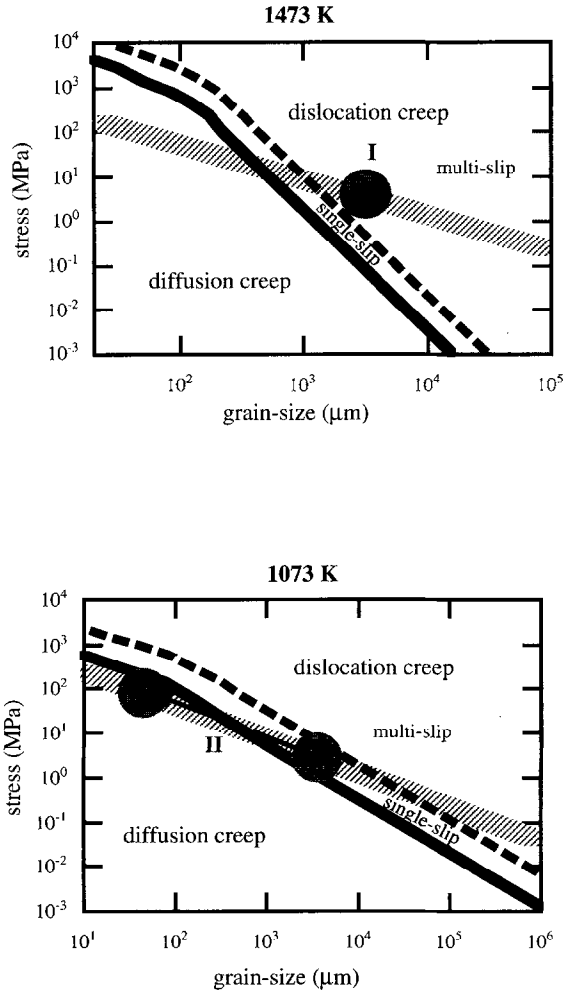

Fig. 10. Deformation mechanism maps for olivine: (a) at 1473 K and (b) at 1073 K. Broken lines indicate the boundaries between multi-slip and single-slip dislocation creep. Solid lines show the boundaries between single-slip dislocation creep and diffusion creep. Deformation is grain-size-sensitive below broken lines (in single-slip dislocation creep and diffusion creep regimes). Dynamic recrystallization occurs in the region above solid lines (experimental data from Karato *et al.*, 1986; Hirth and Kohlstedt, 1995a,b). Thick shaded lines indicate dynamically recrystallized grain size vs stress relationship (Karato *et al.*, 1980; van der Wal *et al.*, 1993). The slight curvature of deformation mechanism boundaries at high stresses is a result of glide-controlled creep operating (Evans and Goetze, 1979). The grain size and stress conditions for stage I and stage II deformation are shown by the shaded regions. Stage II deformation started at a grain size of ~ 3 mm and resulted in a grain size of 30–60 mm. The initial conditions for stage II was a dislocation creep regime (if a boundary for the single-slip control is applied), whereas the final conditions are of a diffusion creep regime.

accommodation needed for deformation by dislocation creep, may play an important role in shear localization in the Earth's upper mantle.

How does this model for shear localization compare with experimental observations? Unfortunately, not many experimental observations are available to constrain the mechanisms of shear localization in upper-mantle peridotites. Post (1977) suggested that dynamic recrystallization might cause shear localization. However, since the mechanical data obtained from the solid-medium Grigg's apparatus are highly unreliable, not much attention has been paid to Post's claim (Post, 1977).

However, the recent study by Zhang *et al.* (submitted), where a high resolution gas-medium deformation apparatus was used, provides experimental observations to support Post's and the present model. Zhang *et al.* (submitted) found that when olivine aggregates are deformed in simple shear, significant strain hardening occurs at 1473 K ($P = 300$ MPa), where little dynamic recrystallization occurs. In contrast, at 1573 K ($P = 300$ MPa), appreciable strain softening is observed associated with dynamic recrystallization. The observation of strain hardening is consistent with the theoretical model by Wenk *et al.* (1991) in which the role of dynamic recrystallization is neglected, and we interpret that this is due to geometrical hardening as opposed to work hardening. The results by Zhang *et al.* (submitted) are therefore consistent with the present model, although the details by which dynamic recrystallization causes softening are not well understood.

Most previous models for shear softening assume that grain-size reduction caused by dynamic recrystallization promotes diffusion creep (Post, 1977; Rutter and Brodie, 1988; Handy, 1989; Drury *et al.*, 1991). These models have a conceptual problem in that dynamic recrystallization is impossible when diffusion creep dominates. This means that softening due to grain-size reduction in such models would work only to an intermediate stage of dynamic recrystallization where a significant volume of a specimen deforms by dislocation creep. Also, if shear localization occurs due to diffusion creep, one should expect to see little LPO in fine recrystallized grains. This is not consistent with observations in shear zones where significant LPO is usually observed in mylonites (e.g. White *et al.*, 1980; see however Behrmann and Mainprice, 1987). Our present model is free from these problems because softening is predicted to occur near the boundary between the two creep mechanisms, where both dislocation and diffusion creep operate. The present model emphasizes the importance of the intermediate regime between dislocation and diffusion creep. In such a regime deformation occurs by dislocation glide, which is accommodated by diffusion creep and/or grain-boundary sliding. Therefore strain rate is sensitive to grain size. Such a regime may be important in materials with a small number of slip systems because strain accommodation plays a key role in determining creep rate in such materials (e.g. Paterson, 1969). This mechanism provides an explanation for the puzzling observation that although shear localization in mylonites is obviously associated with grain-size reduction, rather strong LPO is usually observed in mylonites (e.g. White *et al.*, 1980; Handy, 1989). Further experimental studies on this intermediate regime in crustal rocks, as well as upper-mantle rocks, will be useful to resolve this issue.

When a rock mass undergoes retrograde metamorphism, temperature gradually decreases and stress increases. Therefore, deformation conditions will continuously change from dislocation creep to diffusion creep going through the intermediate regime. Likewise, when continental collision occurs, stress will go up and hence deformation conditions again change from a dislocation creep regime to a diffusion creep regime passing through the intermediate regime. In both cases, deformation in the intermediate regime is unavoidable and will play a critical role in shear localization.

Some previous studies have suggested that shear localization may be due to grain-size reduction associated with some chemical reactions (for a review see Rubie, 1983). Handy (1989) and Drury *et al.* (1991) proposed that shear localization may occur by diffusion creep in the fine-grained layers produced by metamorphic reactions. Similarly, Vissers *et al.* (1995) and Jaroslow *et al.* (1996) suggested grain-size-sensitive flow as a cause of shear localization. Vissers *et al.* (1995) proposed that grain-size reduction was related to syntectonic pyroxene breakdown and the associated ingress of hydrous fluids that resulted in cataclasis. Likewise, Jaroslow *et al.* (1996) invoked high-temperature cataclasis as a cause of grain-size reduction. In these two cases, the proposed physical processes are cataclastic, and a high fluid pressure is implied. In these cases, a conceptual problem of invoking diffusion creep in materials undergoing dynamic recrystallization is not present. Such situations should be possible when thermodynamic conditions are within a certain limited range for relevant reactions to occur. Also, the latter cataclastic mechanisms could occur when a high fluid pressure can be maintained. In contrast to these rather limited conditions, dynamic recrystallization occurs more ubiquitously and perhaps to deeper regions of the upper mantle.

Finally, some comments may be made on the role of grain growth. Although a reduced grain size may cause grain-size-sensitive creep to occur under some conditions, grain growth would make the grain size large enough to terminate this weakening mechanism. This would be the case if weakening and resultant shear localization occur due to the operation of diffusion creep, as proposed in most previous models. In this case, weakening is limited by grain growth. Using the experimental data by Karato (1989b), it is concluded that the weakening will only last for ~ 1–10^2 years at 1000–1200 K, although pinning due to the presence of a secondary phase(s) might prolong this period by reducing grain growth rate. This problem does not occur when weakening occurs by grain-size-sensitive creep in the intermediate regime. In this case continuous grain-size reduction and grain-size-sensitive creep can co-exist, and hence weakening and resultant localization will occur for a much longer period.

Shear localization in the upper mantle

Our analysis shows that deformation in stage I was homogeneous, but deformation in stage II was localized. Why did localized deformation occur in stage II but not in stage I? Under what conditions could shear localiza-

tion through this mechanism occur? How deep in the upper mantle could shear localization occur?

To answer these questions, let us analyze the conditions for shear localization associated with dynamic recrystallization. Rheological behavior associated with dynamic recrystallization (through grain-size effects) is determined by the relationship between recrystallized grain size vs stress curve and the boundary between dislocation and diffusion creep. The former is given by, for example, Karato *et al.* (1980) and Derby and Ashby (1987),

$$d = A(T,\ P,\ C)\sigma^{-p}, \tag{1}$$

where d is grain size, A is a constant that depends on temperature (T), pressure (P) and other parameters characterizing the chemical environment, such as the fugacity of water (C), and p is a constant. Similarly, the boundary between diffusion and dislocation creep is given by,

$$d = B(T,\ P,\ C)\sigma^{-q}, \tag{2}$$

where B is a constant that depends on T, P and C, and q is a parameter that depends on the stress exponent of dislocation creep (n) and grain-size sensitivity of diffusion creep (m) through $q = (n-1)/m$ ($\dot{\epsilon} \sim \sigma^n/d^m$). A recent experimental study suggests that the transition from dislocation to diffusion creep may occur in a more complicated way (Hirth and Kohlstedt, 1995b). Under conditions where contributions from dislocation creep and diffusion creep to strain are comparable, only one easiest slip-system of dislocations ([100](010)) is needed to accommodate deformation (single-slip dislocation creep), whereas when only dislocation glide makes significant contribution to strain, one needs the operation of multiple slip systems (multi-slip dislocation creep). Thus, transition from dislocation creep to diffusion creep occurs taking the following sequence: multi-slip dislocation creep to single-slip dislocation creep and finally to diffusion creep. The boundary between single-slip and multi-slip dislocation creep, however, has not been well constrained. In this paper, an admittedly crude assumption was used that single-slip dislocation creep becomes possible when the contribution to strain from diffusion creep exceeds $\sim 10\%$ of total strain.

The minimum condition for the shear localization is that the size of recrystallized grains is smaller than the size corresponding to the boundary between grain-size-sensitive creep and grain-size-insensitive (multi-slip) dislocation creep (namely broken lines). This condition can be calculated from equations (1) and (2) as,

$$\sigma > \left(\frac{A(T,\ P,\ C)}{B(T,\ P,\ C)}\right)^{\frac{1}{p-q}}. \tag{3}$$

In this paper the experimental results on creep by Karato *et al.* (1986) and Hirth and Kohlstedt (1995a,b), and on dynamic recrystallization by Karato *et al.* (1980) and van der Wal *et al.* (1993), have been used to calculate

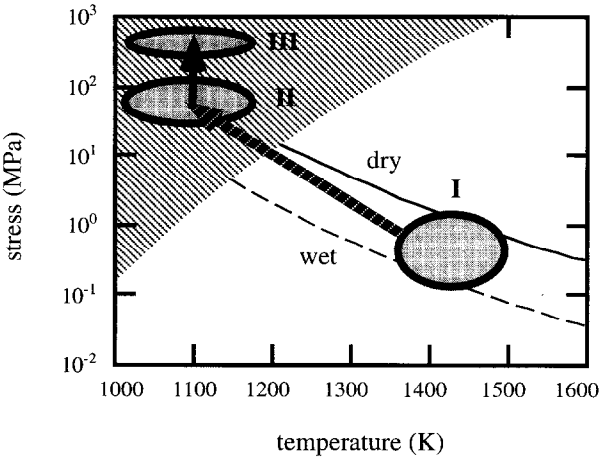

Fig. 11. Conditions for shear localization due to grain-size reduction. The shaded region shows a range of temperature and stress conditions where shear localization occurs by grain-size reduction due to dislocation creep. Shear localization is likely to occur at relatively high stresses and low temperatures. The conditions inferred for stages I, II and III are shown by shaded ellipses. Thin curves show constant strain-rate contours for a strain rate of $10^{-15}\ s^{-1}$ (a solid curve is for dry (water-free) conditions and a broken curve for wet (water-rich) conditions). For this geological strain rate, shear localization will occur when the temperature is lower than $\sim$1100–1200 K, which corresponds to a depth of $\sim$40–80 km for typical geothermal gradients in continents (40–60 mW m^{-2}).

the conditions for shear localization. Both of these experimental studies showed that the effects of water on A and B are small. However, the effects of temperature on the conditions for shear localization are large because the activation energies are different between diffusion and dislocation creep. Shear localization is favored under relatively high stress and low temperatures. To illustrate the probable conditions for shear localization in geological situations equi-strain-rate contours are shown in Fig. 11 for wet (water-rich) and dry (water-free) conditions. For a typical geological strain rate of $\sim 10^{-15}\ s^{-1}$, the threshold temperature for localization is estimated to be $\sim$1200 K for dry conditions and $\sim$1100 K for wet conditions. For a range of reasonable surface heat flow of 40–60 mW m^{-2}, this corresponds to a depth range of 40–80 km.

The estimate of conditions for shear localization shown in Fig. 11 is subject to large uncertainties in relations, such as equations (1) and (2). First, the dynamically recrystallized grain size is usually sensitive mostly to stress magnitude, and is insensitive to temperature and other parameters. However, some theories suggest that dynamically recrystallized grain size might depend on temperature and other thermodynamic conditions (e.g. Derby and Ashby, 1987). The effects of temperature and water on dynamically recrystallized grain size are not well constrained, although the study of Karato *et al.* (1980) and van der Wal *et al.* (1993) showed their effects on dynamic recrystallization to be small. Second, the effects of water on rheology have not been characterized in detail. The effects of water on dynamic recrystallization and creep might be very significant under high-pressure conditions in the Earth's

upper mantle, where water fugacity can be significantly higher than those of experimental studies on recrystallization and creep performed so far (Karato *et al.*, 1980, 1982, 1986; Hirth and Kohlstedt, 1995a,b, 1996; Kohlstedt *et al.*, 1996). Third, both recrystallized grain size and creep laws were determined at relatively high temperatures. Extrapolation of these data to significantly lower temperatures causes large uncertainties because dominant slip systems are known to be different under low-temperature conditions, which probably affects rheology and recrystallized grain size. Therefore our mechanism for shear localization should be considered tentative until more detailed experimental studies are performed on these parameters.

Although the conditions for shear localization are limited to relatively high stresses and low temperatures, localization is likely to occur close to the depth at which the strength–depth profile has a maximum (Goetze and Evans, 1979), where much of the load is supported. Therefore, shear localization should play an important role in reducing the strength of the lithosphere. Once localized deformation occurs, then rheology in that region will be significantly softer than expected from the simple extrapolation of grain-size-insensitive rheology. Furthermore, such enhanced deformation could trigger thermal runaway to cause the very fast deformation responsible for earthquakes (Obata and Karato, 1995). These rheological complexities should be incorporated into realistic modeling of deformation of the lithosphere, particularly during continental collisions.

Acknowledgements—Gilles Bussod made important contributions to the fieldwork carried out in 1993 and some microstructural analysis. We thank Shuqing Zhang and Zichao Wang for technical assistance. Detailed constructive criticisms by Martyn Drury and Greg Hirth greatly helped to improve the paper. This study was supported by National Science Foundation (U.S.A.) through the grant EAR-9220172.

REFERENCES

Behrmann, J. H. and Mainprice, D. (1987) Deformation mechanisms in a high-temperature quartz–feldspar mylonite: evidence for superplastic flow in the lower continental crust. *Tectonophysics* **140**, 297–305.

Boudier, F., Jackson, M. and Nicolas, A. (1984) Structural study of the Balmuccia massif (Western Alps): a transition from mantle to lower crust. *Geologie en Mijnbouw* **63**, 179–188.

Brodie, K. H. and Rutter, E. H. (1987) Deep crustal extensional faulting in the Ivrea zone of northern Italy. *Tectonophysics* **140**, 193–212.

Coe, R. S. and Kirby, S. H. (1975) The orthoenstatite to clinoenstatite transformation by shearing and reversion by annealing: mechanism and potential applications. *Contributions to Mineralogy and Petrology* **52**, 29–55.

Derby, B. and Ashby, M. F. (1987) On dynamic recrystallization. *Scripta Metallica* **21**, 879–884.

Drury, M. R., Vissers, R. L. M., van der Wal, D. and Hoogerduijn Strating, E. H. (1991) Shear localization in upper mantle peridotites. *Pure and Applied Geophysics* **137**, 439–460.

Durham, W. B., Ricoult, D. L. and Kohlstedt, D. L. (1985) Interaction of slip systems in olivine. In *Point Defects in Minerals*, ed. R. N. Schock, pp. 185–193. American Geophysical Union, Washington, DC.

Evans, B. and Goetze, C. (1979) Temperature variation of hardness of olivine and its implication for polycrystalline yield stress. *Journal of Geophysical Research* **84**, 5505–5524.

Goetze, C. and Evans, B. (1979) Stress and temperature in the bending lithosphere as constrained by experimental rock mechanics. *Geophysical Journal of the Royal Astronomical Society* **59**, 463–487.

Handy, M. R. (1989) Deformation regimes and rheological evolution of fault zone in the lithosphere: the effects of pressure, temperature, grain-size and time. *Tectonophysics* **163**, 119–152.

Handy, M. R. (1994) Flow laws for rocks containing two non-linear viscous phases: a phenomenological approach. *Journal of Structural Geology* **16**, 287–301.

Harren, S. V., Deve, H. E. and Asaro, R. J. (1988) Shear band formation in plane compression. *Acta Metallica* **36**, 2435–2480.

Hirth, G. and Kohlstedt, D. L. (1995) Experimental constraints on the dynamics of partially molten upper mantle: deformation in the diffusion creep regime. *Journal of Geophysical Research* **100**, 1981–2001.

Hirth, G. and Kohlstedt, D. L. (1995) Experimental constraints on the dynamics of partially molten upper mantle: deformation in the dislocation creep regime. *Journal of Geophysical Research* **100**, 15441–15449.

Hirth, G. and Kohlstedt, D. L. (1996) Water in the oceanic upper mantle: implications for rheology, melt extraction and the evolution of the lithosphere. *Earth and Planetary Science Letters* **144**, 93–108.

Hobbs, B. E., Ord, A. and Teyssier, C. (1986) Earthquakes in the ductile regime? *Pure and Applied Geophysics* **124**, 309–336.

Jaroslow, G. E., Hirth, G. and Dick, H. J. B. (1996) Abyssal peridotite mylonites: implications for grain-size sensitive flow and strain localization in the oceanic lithosphere. *Tectonophysics* **256**, 17–37.

Jordan, T. H. (1975) The continental tectosphere. *Review of Geophysics and Space Physics* **13**, 1–12.

Kamb, W. B. (1959) Ice petrofabric observation from Blue glacier, Washington, in relation to theory and experiment. *Journal of Geophysical Research* **64**, 155–176.

Karato, S. (1987) Scanning electron microscope observation of dislocations in olivine. *Physics and Chemistry of Minerals* **14**, 245–248.

Karato, S. (1988) The role of recrystallization in lattice preferred orientation in olivine. *Physics of Earth and Planetary Interiors* **51**, 108–122.

Karato, S. (1989a) Seismic anisotropy: mechanisms and tectonic implications. In *Rheology of Solids and of the Earth*, ed. S. Karato and M. Toriumi, pp. 393–422. Oxford University Press, Oxford.

Karato, S. (1989b) Grain-growth kinetics in olivine aggregates. *Tectonophysics* **168**, 255–273.

Karato, S., Paterson, M. S. and FitzGerald, J. D. (1986) Rheology of synthetic olivine aggregates: influence of grain size and water. *Journal of Geophysical Research* **91**, 8151–8176.

Karato, S., Toriumi, M. and Fujii, T. (1980) Dynamic recrystallization of olivine single crystals during high temperature creep. *Geophysical Research Letters* **7**, 649–652.

Karato, S., Toriumi, M. and Fujii, T. (1982) Dynamic recrystallization and high temperature rheology of olivine. In *High Pressure Research in Geophysics*, ed. S. Akimoto and M. H. Manghnani, pp. 171–189. Center for Academic Press, Tokyo.

Kohlstedt, D. L., Evans, B. and Mackwell, S. J. (1995) Strength of the lithosphere: constraints imposed by laboratory experiments. *Journal of Geophysical Research* **100**, 17587–17602.

Kohlstedt, D. L. and Goetze, C. (1974) Low-stress high-temperature creep of olivine single crystals. *Journal of Geophysical Research* **85**, 6269–6285.

Kohlstedt, D. L., Keppler, H. and Rubie, D. C. (1996) Solubility of water in the α, β, γ phases of $(Mg,Fe)_2SiO_4$. *Contributions to Mineralogy and Petrology* **123**, 345–357.

Luton, M. J. and Sellars, S. M. (1969) Dynamic recrystallization in nickel and nickel iron alloys during high temperature deformation. *Acta Metallica* **17**, 1033–1043.

Nicolas, A. and Christensen, N. I. (1987) Formation of anisotropy in upper mantle peridotites: A review. In *Composition, Structure and Dynamics of the Lithosphere/Asthenosphere System*, ed. K. Fuchs and C. Froidevaux, pp. 111–123. American Geophysical Union, Washington, DC.

Obata, M. and Karato, S. (1995) Ultramafic pseudotachylyte from Ivrea–Verbano zone, northern Italy. *Tectonophysics* **242**, 313–328.

Paterson, M. S. (1969) The ductility of rocks. In *Physics of Strength and Plasticity*, ed. A. S. Argon, pp. 377–392. MIT Press, Cambridge, Massachusetts.

Paterson, M. S. (1978) *Experimental Rock Deformation: The Brittle Field*. Springer, Berlin.

Peltier, W. R. (1984) The thickness of the continental lithosphere. *Journal of Geophysical Research* **89**, 11303–11316.

Poirier, J.-P. (1980) Shear localization and shear instability in materials in the ductile field. *Journal of Structural Geology* **2**, 135–142.

Poirier, J.-P. and Nicolas, A. (1975) Deformation-induced recrystallization by progressive misorientation of subgrain-boundaries, with special reference to mantle peridotites. *Journal of Geology* **83**, 707–720.

Post, R. L. (1977) High-temperature creep of Mt. Burnett dunite. *Tectonophysics* **42**, 75–110.

Rubie, D. C. (1983) Reaction enhanced ductility: the role of solid-state univariant reactions in the deformation of the crust and mantle. *Tectonophysics* **96**, 331–352.

Rutter, E. H. and Brodie, K. H. (1988) The role of tectonic grain-size reduction in the rheological stratification of the lithosphere. *Geologische Rundschau* **77**, 295–308.

Rutter, E. H. and Brodie, K. H. (1990) Some geophysical implications of the deformation and metamorphism of the Ivrea zone, northern Italy. *Tectonophysics* **182**, 147–160.

Rutter, E. H., Brodie, K. H. and Evans, P. J. (1993) Structural geometry, lower crustal magmatic underplating and lithospheric stretching in the Ivrea–Verbano zone, northern Italy. *Journal of Structural Geology* **15**, 647–662.

Schmid, R. and Wood, B.J. (1976) Phase relationships in granulitic metapelites from the Ivrea–Verbano Zone (N. Italy). *Contributions to Mineralogy and Petrology* **54**, 255–279.

Shervais, J. W. (1979) Thermal emplacement model for the Alpine lherzolite massif at Balmuccia, Italy. *Journal of Petrology* **20**, 795–820.

Sibson, R. H. (1975) Generation of pseudotachylite by ancient seismic faulting. *Geophysical Journal of the Astronomical Society* **43**, 775 794.

Skrotzki, W., Wedel, A., Weber, K. and Müller, W. F. (1990) Microstructure and texture in lherzolites of the Balmuccia massif and their significance regarding the thermomechanical history. *Tectonophysics* **179**, 227–251.

Techmer, K. S., Ahrendt, H. and Weber, K. (1992) The development of pseudotachylyte in the Ivrea–Verbano zone of the north Italian Alps. *Tectonophysics* **204**, 307–322.

van der Wal, D., Chopra, P. N., Drury, M. and FitzGerald, J. D. (1993) Relationships between dynamically recrystallized grain size and deformation conditions in experimentally deformed olivine rocks. *Geophysical Research Letters* **20**, 1479–1482.

Vissers, R. L. M., Drury, M. R., Hoogerduijn Strating, E. H., Spiers, C. J. and van der Wal, D. (1995) Mantle shear zones and their effects on lithosphere strength during continental breakup. *Tectonophysics* **249**, 155–171.

Wenk, H.-R., Bennett, K., Canova, G. R. and Molinari, A. (1991) Modelling plastic deformation of peridotite with the self-consistent theory. *Journal of Geophysical Research* **96**, 8337–8349.

White, S. H., Burrows, S. E., Shaw, N. D. and Humphreys, F. J. (1980) On mylonites in ductile shear zones. *Journal of Structural Geology* **2**, 175–189.

Zeuch, D. H. (1982) Ductile faulting, dynamic recrystallization and grain size sensitive flow of olivine. *Tectonophysics* **83**, 293–308.

Zhang, S. and Karato, S. (1995) Lattice preferred orientation of olivine deformed in simple shear. *Nature* **375**, 774–777.

Zingg, A., Handy, M. R., Hunziker, J. C. and Schmid, S. M. (1990) Tectonometamorphic history of the Ivrea zone and its relationship to the crustal evolution of the south Alps. *Tectonophysics* **182**, 169–192.